Mesoporous Materials

DOI: 10.1002/ange.201305819

Surface-Metastable Phase-Initiated Seeding and Ostwald Ripening: A Facile Fluorine-Free Process towards Spherical Fluffy Core/Shell, Yolk/Shell, and Hollow Anatase Nanostructures**

Lu Cao, Dehong Chen, and Rachel A. Caruso**

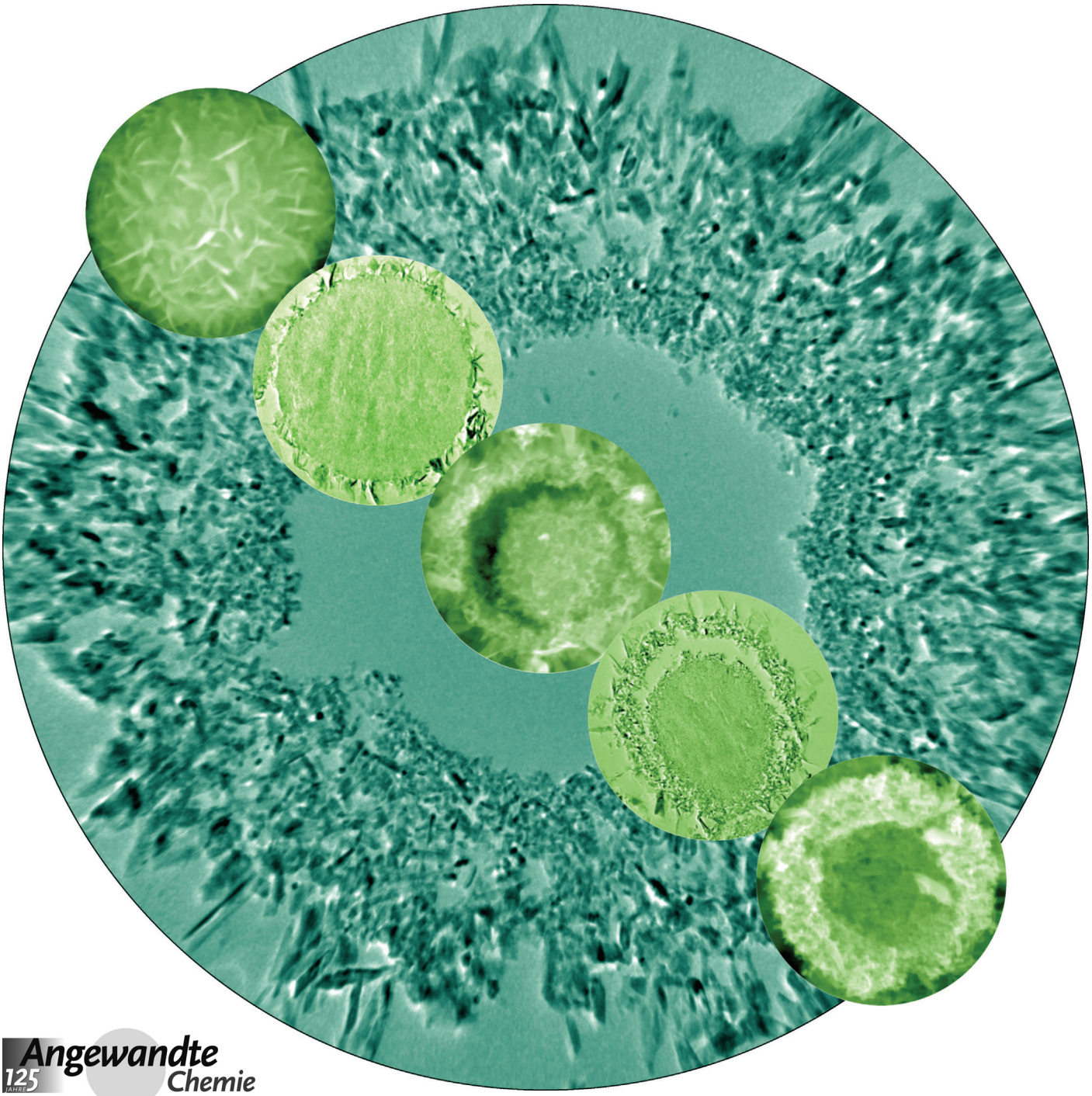

WILEY ONLINE LIBRARY

© 2013 Wiley-VCH Verlag GmbH & Co. KGaA, Weinheim

A wide variety of hollow inorganic nanostructures have received recent attention because of their promising applications including drug delivery, photocatalytic redox reactions and water splitting, clean energy conversion and storage, gas sensing, and heavy-metal ion sequestration.[1] Significant effort has been dedicated to developing facile and effective approaches for the fabrication of various hollow structures with sophisticated architectures and varied compositions.[1a–d,2] Among the diverse synthesis approaches (e.g. templating synthesis, Kirkendall diffusion process, Galvanic replacement method), Ostwald ripening,[2f,g,3] a well-known physical phenomenon, has recently shown great versatility for the generation of diverse hollow inorganic crystalline structures on micro-/submicrometer scales.[2f,g,4] For this approach, it is generally believed that the central crystallites with relatively small sizes would have a strong tendency to dissolve into solution, and then be subsequently relocated to the particle surface by a recrystallization process, thus giving rise to nanostructures with hollow interior spaces. The ultimate architecture of the interior space highly depends on the packing of the initial crystalline aggregates prior to the Ostwald ripening process.[2f,g]

Although this template-free Ostwald ripening approach has explained the fabrication of numerous different hollow materials,[2f,g,3–5] direct evidence in support of this formation mechanism is lacking because most research investigated these hollow structures using conventional mass/thickness contrast obtained using TEM.[2f,g,3,4] Because of the relatively large size (usually >200 nm) of the nanostructures and the overlap of the shell from both sides of the sample in the image, the detailed architecture (e.g. crystal size, morphology, uniformity, packing manner, porosity and thickness) of the shell layers could not be resolved using conventional TEM characterization. Thus, unambiguous evidence relating to the seeding (formation of crystalline nanoparticles on the surfaces), crystal growth through Ostwald ripening (formation of larger crystals at the expense of smaller counterparts) and the subsequent hollowing process has not been available.

As an important material with numerous practical applications and industrial interest, titania has attracted significant attention since its commercial production in the early 20th century.[6] The Ostwald ripening process has been applied to synthesize diverse hollow titania nanostructures,[2f,g,4a,b,5] however, the fabrication process usually involves the participation of various fluorides (e.g. TiF_4),[4a,b,5] which produces highly corrosive and toxic hydrofluoric acid (HF) during the synthesis. Extra care and protection is essential in handling HF acid, thus decreasing the practicality of this synthesis approach. Therefore a fluorine-free and effective process for the fabrication of diverse hollow titania nanostructures would be desirable, especially for the potential large-scale production of these nanostructures. We demonstrate herein a facile and versatile fluorine-free solvothermal process to fabricate anatase nanostructures with diverse sophisticated morphologies, including spherical "fluffy" core/shell, yolk/shell, and hollow nanostructures. A metastable phase on the surface of the spheres initiated seeding and the Ostwald ripening process, as determined from a range of characterization techniques that revealed the morphological evolution and crystallization process occurred in the presence of an ammonia solution.

These nanostructures were synthesized using a facile one-pot solvothermal crystallization process featuring three stepwise reaction stages as shown in Scheme 1. The experimental details of the synthesis and characterization of these samples can be found in the Supporting Information. This solvothermal crystallization proceeded in the presence of 21.3 wt% ammonia solution within an autoclave heated at 160 °C and no fluorine species were required during the synthesis. After calcination at temperatures over 500 °C in air, the amorphous titania cores of the intermediates can be readily converted into particulate anatase counterparts without damaging the overall morphologies, thus enabling a facile and scalable approach for fabricating spherical "fluffy" core/shell, yolk/shell, and hollow anatase nanostructures.

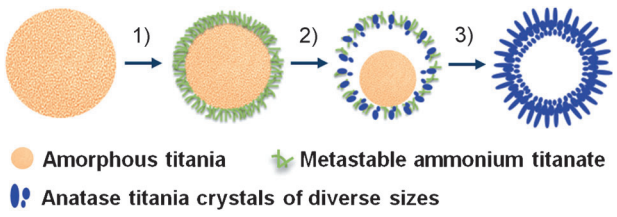

Scheme 1. Formation process of diverse titania/titanate nanostructures: 1) precipitation of a metastable phase, ammonium titanate nanoflakes, on the surfaces of amorphous titania microspheres using an energy-favored heteronucleation process, producing a "fluffy" core/shell-structured intermediate; 2) phase transformation of the metastable ammonium titanate nanoflakes to anatase nanocrystals occurred in the shell layer of the intermediate microsphere whereas the core remained amorphous, which subsequently initiated an Ostwald ripening process and gave rise to the yolk/shell nanostructures; and 3) formation of self-supported porous shells consisting of faceted anatase nanocrystals with a gradient in size using the Ostwald ripening process.

[*] L. Cao, Dr. D. H. Chen, Prof. R. A. Caruso
Particulate Fluids Processing Centre, School of Chemistry
The University of Melbourne
Victoria 3010 (Australia)
E-mail: dehongc@unimelb.edu.au
rcaruso@unimelb.edu.au
Prof. R. A. Caruso
CSIRO Materials Science and Engineering
Private Bag 33, Clayton South, Victoria 3169 (Australia)

[**] This research was financially supported by an Australian Research Council Discovery Project (grant number DP110101346). L.C. acknowledges the support of an Australian Postgraduate Award and MMI-CSIRO PhD Materials Science Top-up. R.A.C. is a recipient of an Australian Research Council Future Fellowship (grant number FT0990583). Dr. Simon Crawford is thanked for ultramicrotoming samples in preparation for TEM characterization. Dr. Xiaofei Duan and Mr David Parris are appreciated for acquiring XPS and XRD results, respectively. The Advanced Microscopy Facility and Surface and Chemical Analysis Network (SCAN) at the University of Melbourne are acknowledged for electron microscopy and XPS access, respectively.

Supporting information for this article is available on the WWW under http://dx.doi.org/10.1002/anie.201305819.

 © 2013 Wiley-VCH Verlag GmbH & Co. KGaA, Weinheim

To illustrate the formation mechanism of these titania nanostructures, an investigation using SEM, TEM, XRD, and thermogravimetric/differential thermal analysis (TGA/DTA) was conducted to monitor the morphological evolution and crystallization process as a function of the solvothermal treatment time. SEM images of the precursor microspheres and the solvothermally treated counterparts (prior to calcination) at varied intervals (0, 16, 24, and 48 h) are shown in Figure 1. In conjunction with the SEM images showing detailed surface features of the microspheres, these samples

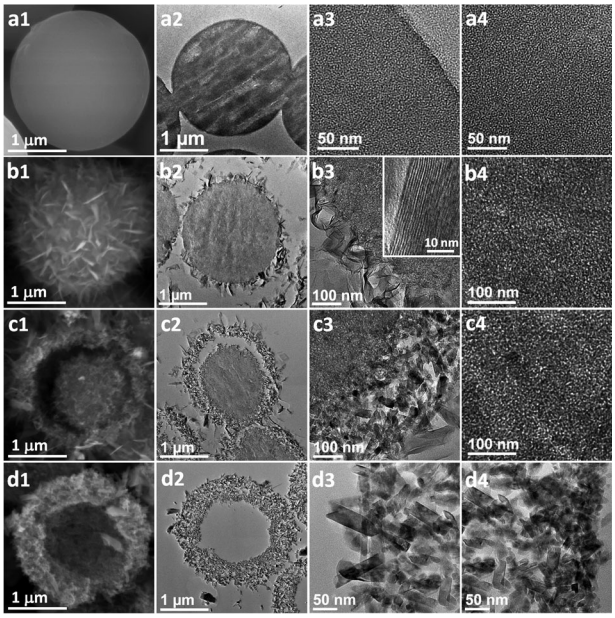

Figure 1. SEM and TEM (ultramicrotomed sections) images of the amorphous precursor microspheres (a1–a4) and solvothermally treated titania microspheres (prior to calcination) obtained with varying solvothermal times: 16 h for amorphous titania/ammonium titanate core/shell structures (b1–b4, the inset in b3 shows a high-resolution TEM image of the ammonium titanate nanosheets); 24 h for amorphous titania/anatase yolk/shell structures (c1–c4); and 48 h for anatase hollow microspheres (d1–d4). Images shown in a3, b3, and c3 and those in a4, b4, and c4 display the edge and the core sections of the titania microspheres, respectively. d3 and d4 images show parts of the outer and inner shell of the anatase hollow structure, respectively. Note: SEM images were taken without sputter coating.

were ultramicrotomed to about 90 nm thick sections and analyzed using TEM to investigate the porous shells and interior core structures. Precursor microspheres possess fairly smooth surfaces (Figure 1 a1 and Figure S1a in the Supporting Information), indicating they consist of ultrafine primary particles. These precursor microspheres have wormhole-like mesostructures throughout the whole particle (Figure 1 a3 surface and 1 a4 core) and are amorphous at atomic scale as identified by the corresponding XRD pattern (Figure S1m) and diffuse selected-area electron diffraction (SAED) pattern (Figure S2a). After solvothermal treatment at 160 °C for 2 h, microspheres covered with a few thin sheetlike nanostructures are observed (Figure S1c,d). The corresponding XRD pattern demonstrates that these microspheres are still amorphous (Figure S1m). Progressively more sheetlike nanostructures formed on the surfaces of the microspheres when prolonging the solvothermal time to 4 and 16 h (Figure S1e–h). After 4 h, an obvious diffraction peak around $2\theta = 9.8°$ appeared in the corresponding XRD pattern (Figure S1m). By further increasing the solvothermal treatment time to 16 h, this low-angle diffraction peak became more distinct along with the appearance of three other diffraction peaks around $2\theta = 27.6$, 48.1, and 62.9°. All these diffraction peaks are associated with the sheetlike nanostructures covered on the surfaces of the microspheres and can be ascribed to the formation of ammonium titanate,[7] a lamellar titanate intercalated with ammonium cations between TiO_6 octahedra layers. For the microspheres solvothermally treated for 16 h (Figure 1 b1), a "fluffy" amorphous titania/ammonium titanate core/shell nanostructure was obtained. The corresponding SEM and TEM images (Figure 1 b1, 1 b2, and 1 b3) clearly show that the titanate nanoflakes are attached to the surfaces of the spherical particle. These nanosheets have an interlayer spacing of about 0.80 nm (inset in Figure 1 b3), which is close to the interplanar distance of the (200) plane of the ammonium titanate,[7b] further confirming the formation of such a metastable intermediate phase. As shown in Figure 1 b4, this "fluffy" core/shell nanostructure possessed an amorphous core featuring the wormholelike mesostructure. With increased reaction time (24 h), shown in Figure 1 c1 and 1 c2, the cores shrank, producing unique yolk/shell nanostructures. Such yolk/shell nanostructures possess an intermeshed particulate shell consisting of both ammonium titanate nanosheets and anatase nanocrystals (Figure 1 c1–c3), while retaining a mesostructured amorphous yolk (Figure 1 c4). The crystal phase of these yolk/shell nanostructures was determined by the corresponding XRD pattern (Figure S1m), in which a reduced peak intensity in ammonium titanate phase and the occurrence of additional diffraction peaks around $2\theta = 25.6$, 38.1, 48.1, and 62.9° are observed. These newly appearing peaks can be indexed to the (101), (004), (200), and (204) planes of the anatase titania, respectively, indicating the occurrence of a gradual phase transformation from ammonium titanate to anatase titania.[7c] Further increasing the solvothermal treatment to 48 h gives rise to anatase microspheres with completely hollow interiors (Figure 1 d1, 1 d2, and Figure S1k). These hollow microspheres have a porous shell of about 550 nm in thickness and an inner cavity of about 1200 nm in diameter. The shells are mainly composed of faceted rodlike nanocrystals with a length ranging from 10 to 300 nm, and relatively small anatase crystals primarily gathered on the inner surfaces of the hollow spheres. The corresponding XRD pattern (Figure S1 m) revealed that these nanocrystals are well-crystallized anatase-phase titania.

The presence of amorphous titania in the core regions of the microspheres solvothermally treated for less than 24 h is also supported by the corresponding DTA results (Figure S3a). The sharp exothermic peaks centered at 472 °C, which can be mainly ascribed to the crystallization from amorphous to anatase titania,[8] were clearly observed for the microspheres solvothermally treated for 2 and 16 h. This exothermic peak became less defined for the microspheres

© 2013 Wiley-VCH Verlag GmbH & Co. KGaA, Weinheim

solvothermally treated for 24 h because of the decrease in the amorphous titania core content. When prolonging the solvothermal time to 48 h, no obvious exothermic peak was observed on the corresponding DTA curve (Figure S3a), suggesting that the amorphous phase in these microspheres has been fully converted to anatase during the solvothermal crystallization. The overall weight loss of the solvothermally treated samples decreased with increasing solvothermal treatment time as shown in the TGA curves (Figure S3b). This indicates that the microspheres gradually became less hydrated and the organic residue content decreased with increasing solvothermal treatment time.

The above SEM, TEM, XRD, and TGA-DTA results clearly indicate that 1) sheetlike ammonium titanate, an intermediate phase, formed and kept growing on the outer surfaces of the microspheres during the early stage (<16 h) of the solvothermal process, 2) being a metastable phase, this ammonium titanate can be readily transformed into anatase with further solvothermal heating (≥ 24 h), and 3) the anatase nanocrystals formed on the shell layers of the spherical particles acted as the seeds and initiated the well-known Ostwald ripening process towards the formation of hollow anatase microspheres. This is different to most of the previous published articles in which the hollowing process is generally suggested to start from the center of the spherical particles.[2f,g,4a] The hollowing process, as evidenced by the TEM images of the ultramicrotomed sample sections, occurred initially from the surfaces just underneath the crystalline shell layer and it proceeded inwardly at the expense of the interior amorphous core.

To understand the role of ammonia in the formation of these hollow titania nanostructures, a control experiment was conducted by replacing the ammonia solution with water under otherwise identical conditions. As shown in Figure S4a–m, the resulting microspheres were composed of ultrafine anatase nanocrystals. The high-magnification TEM images (Figure S4e,f or k, l) indicate that the nanocrystals are nearly identical in size throughout the whole particle when ammonia was not present. Because of the absence of obvious difference in crystal size between the shell layers and the core regions of these microspheres, the Ostwald ripening process was less likely to be trigged to form the hollow spheres in this case.

The "fluffy" core/shell intermediates (solvothermally treated for 16 h) and the yolk/shell nanostructures (solvothermally treated for 24 h) can be readily converted to anatase counterparts without changing the overall morphologies during calcination. Figure 2 displays SEM and TEM images of these anatase nanostructures calcined at 650 °C for 2 h in air. "Fluffy" core/shell anatase nanostructures (Figure 2 a,b and Figure S5a,b) were covered by thin sheetlike nanostructures on the outer surfaces. As illustrated by a broken microsphere, Figure S5b, the core of the microsphere is composed of granular nanocrystals. This result is also confirmed by the corresponding TEM images shown in Figure S5c and S5d, in which a homogeneous particulate network consisting of about 20 nm crystals is clearly observed throughout the whole core of the sliced sample. Elongated nanocrystals surrounding this core (Figure S5c) correspond to

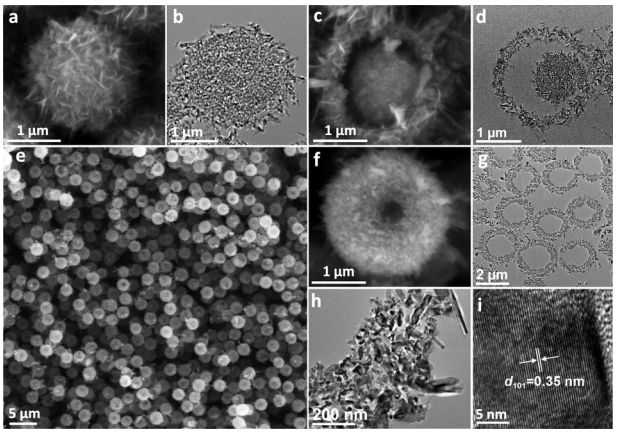

Figure 2. SEM and TEM (ultramicrotomed sections) images of the calcined "fluffy" core/shell anatase microspheres (a, b, Solvo-16 h-Cal), yolk/shell anatase microspheres (c, d, Solvo-24 h-Cal) and hollow anatase microspheres (e–i, Solvo-48 h-Cal), i) high resolution TEM images of a typical rodlike nanocrystal indicating its high crystallinity and oriented elongation along the [001] direction. Note: SEM images were taken without sputter coating.

the sheetlike nanostructures. Anatase nanostructures with yolk/shell structure are shown in Figure 2 c and 2 d. In this case, the shells consist of a mixture of sheetlike and elongated nanocrystals (Figure 2 c and Figure S6), while the yolks are spherical assemblies of nanocrystals (Figure 2 d). The resulting nanostructures are monodisperse entities, for example, the hollow anatase microspheres (shown in Figure 2 e) possess an average diameter of 2.3 ± 0.1 μm based on analysis of 240 entities (shown in Figure S7). A typical high-magnification SEM image, as shown in Figure 2 f, clearly reveals the rough surface feature and the presence of a void (about 380 nm in diameter) on the surface. As confirmed by the corresponding TEM analysis (Figure 2 g), these titania microspheres possess hollow chambers and uniform shells of about 550 nm in thickness (Figure 2 g and h). The shells are mainly composed of faceted rodlike nanocrystals with a length ranging from 10 to 300 nm. The corresponding high-resolution TEM image (Figure 2 i) shows continuous lattice fringes throughout the whole nanocrystal to the edges, indicating a high crystallinity of the products. Spacing between the lattice fringes of the nanocrystals was measured to be 0.35 nm, which corresponds to the spacing of (101) planes of the anatase phase (JCPDS card No. 21-1272), indicating an oriented elongation of the crystal along the [001] direction.

XRD studies were carried out to investigate the crystal phase and crystallinity of these calcined products. As illustrated in Figure S8a, XRD patterns of these calcined microspheres can be assigned to the anatase phase of titania. The diffraction peaks become sharper when the solvothermal treatment time was prolonged from 16 to 24 h, and to 48 h, indicating formation of larger anatase crystals with enhanced crystallinity by increasing the solvothermal treatment time. An X-ray photoelectron spectroscopy (XPS) survey and high-resolution spectra analysis were performed to further investigate surface compositions and crystallinity of the resulting nanostructures (Figure S8b and S9). The high-resolution Ti2p

 © 2013 Wiley-VCH Verlag GmbH & Co. KGaA, Weinheim

XPS spectra shown in Figure S8b further confirming an enhanced crystallinity of the resulting products.[9]

The photocatalytic activity of these calcined microspheres was evaluated by the photodegradation of methylene blue (MB), a probe molecule, under UV light irradiation. For comparison, the photocatalytic activity of nanoparticles of Degussa P25, a well-known highly efficient titania photocatalyst, was also measured under the same conditions. Figure S10 represents a time profile of the MB absorption spectra recorded in the presence of hollow anatase microspheres exposed to UV light. To compare the reaction kinetics of the MB degradation, a pseudo-first-order reaction rate equation was used ($\ln(C/C_0) = k\,t$, where C and C_0 refer to the concentration of MB at the irradiation time t and 0 minutes, k and t are the reaction rate constant and photodegradation time, respectively). As shown in Figure 3, the plots are linear

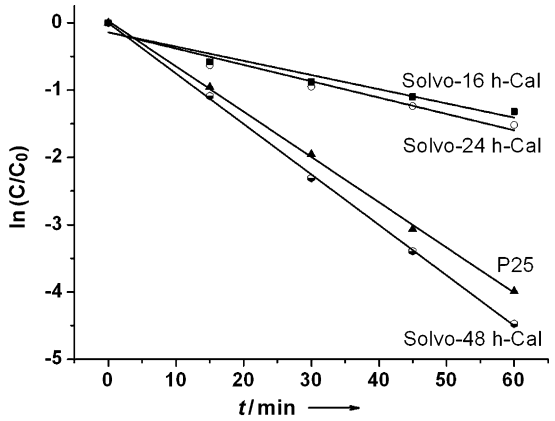

Figure 3. Photocatalytic degradation of methylene blue in the presence of calcined "fluffy" core/shell anatase microspheres, yolk/shell anatase microspheres, hollow anatase microspheres, and Degussa P25 nanoparticles.

indicating a fit with the pseudo-first-order reaction kinetics, and the degradation of MB improved with increasing solvothermal treatment time (from 16 to 48 h). The hollow anatase microspheres show a much higher degradation rate ($k = 0.0750\ \text{min}^{-1}$) than those microspheres with either "fluffy" core/shell structure (Solvo-16 h-Cal, $k = 0.0211\ \text{min}^{-1}$) or yolk/shell structure (Solvo-24 h-Cal, $k = 0.0243\ \text{min}^{-1}$). The hollow anatase microspheres display higher photocatalytic performance than that of the Degussa P25 nanoparticles ($k = 0.0673\ \text{min}^{-1}$) even though these hollow microspheres possess lower surface area ($41\ \text{m}^2\,\text{g}^{-1}$, Figure S11) compared to that of the Degussa P25 ($50\ \text{m}^2\,\text{g}^{-1}$). UV/Vis diffuse reflectance spectra and plots of the Kubelka–Munk function (i.e., relationship of $[F(R)h\nu]^{1/2}$ versus photon energy) to determine the bandgaps of these titania photocatalysts are shown in Figure S12a and S12b. The anatase microspheres have relatively narrow bandgaps (3.25 eV for Solvo-16 h-Cal and Solvo-24 h-Cal and 3.27 eV for Solvo-48 h-Cal sample) compared with the Degussa P25 nanoparticles (3.36 eV). Among the above titania photocatalysts, the hollow anatase microspheres possesses the lowest surface area ($41\ \text{m}^2\,\text{g}^{-1}$), however, this sample presents the best photocatalytic activity. The superior photocatalytic activity of these anatase hollow structures could be speculated to be due to the following synergistic effects: 1) the unique hollow structure could cause multireflection of the light once the incident light has entered into the interior spherical chamber (like a spherical integrating chamber), thus maximizing the light harvesting and utilization efficiency;[10] 2) the hierarchically porous shells provide numerous diffusion paths for the pollutants to travel throughout the material and promote accessibility to the active surface sites;[11] 3) the intermeshed networks of the shells and enhanced crystallinity, as confirmed by corresponding XRD, XPS, and HRTEM results, could reduce the recombination rate of the photogenerated electrons and holes and prolong the electron lifetimes and diffusion lengths, therefore improving the overall photocatalytic activity.[6d,12]

In summary, a versatile fluorine-free approach has been demonstrated for structural and morphological engineering of anatase nanomaterials and gave rise to spherical "fluffy" core/shell, yolk/shell, and hollow anatase nanostructures using a facile one-pot solvothermal process. The ammonia present in the synthesis solution retarded the direct crystallization from amorphous titania to anatase nanocrystals and promoted the formation of metastable ammonium titanate nanoflakes on the surfaces of the precursor particles. The anatase nanocrystals derived from the ammonium titanate intermediates on the surface acted as the seeds and initiated the Ostwald ripening process, and thus gave rise to anatase nanostructures with diverse complex morphologies. The resulting hollow anatase microspheres showed an enhanced photocatalytic activity over the commercial P25 nanoparticles. It is believed that this novel surface-based, metastable phase-mediated synthesis strategy could be extended to the fabrication of a wide variety of functional hollow nanostructures with diverse composition or morphologies in future.

Received: July 5, 2013
Published online: August 23, 2013

Keywords: mesoporous materials · nanostructures · photochemistry · solvothermal synthesis · titanates

[1] a) X. W. Lou, L. A. Archer, Z. C. Yang, *Adv. Mater.* **2008**, *20*, 3987 – 4019; b) J. Hu, M. Chen, X. S. Fang, L. W. Wu, *Chem. Soc. Rev.* **2011**, *40*, 5472 – 5491; c) X. Lai, J. Li, B. A. Korgel, Z. Dong, Z. Li, F. Su, J. Du, D. Wang, *Angew. Chem.* **2011**, *123*, 2790 – 2793; *Angew. Chem. Int. Ed.* **2011**, *50*, 2738 – 2741; d) L. Zhou, D. Y. Zhao, X. W. Lou, *Angew. Chem.* **2012**, *124*, 243 – 245; *Angew. Chem. Int. Ed.* **2012**, *51*, 239 – 241; e) X. M. Sun, Y. D. Li, *Angew. Chem.* **2004**, *116*, 3915 – 3919; *Angew. Chem. Int. Ed.* **2004**, *43*, 3827 – 3831.

[2] a) Y. G. Sun, Y. N. Xia, *Science* **2002**, *298*, 2176 – 2179; b) Y. G. Sun, B. T. Mayers, Y. N. Xia, *Nano Lett.* **2002**, *2*, 481 – 485; c) Y. D. Yin, R. M. Rioux, C. K. Erdonmez, S. Hughes, G. A. Somorjai, A. P. Alivisatos, *Science* **2004**, *304*, 711 – 714; d) F. Caruso, R. A. Caruso, H. Mohwald, *Science* **1998**, *282*, 1111 – 1114; e) Q. Zhang, W. S. Wang, J. Goebl, Y. D. Yin, *Nano Today* **2009**, *4*, 494 – 507; f) H. C. Zeng, *J. Mater. Chem.* **2011**, *21*, 7511 – 7526; g) H. C. Zeng, *Curr. Nanosci.* **2007**, *3*, 177 – 181; h) Y.

 © 2013 Wiley-VCH Verlag GmbH & Co. KGaA, Weinheim

Chen, H. Chen, L. Guo, Q. He, F. Chen, J. Zhou, J. Feng, J. Shi, *ACS Nano* **2010**, *4*, 529 – 539.
[3] D. P. Wang, H. C. Zeng, *Chem. Mater.* **2011**, *23*, 4886 – 4899.
[4] a) H. G. Yang, H. C. Zeng, *J. Phys. Chem. B* **2004**, *108*, 3492 – 3495; b) J. H. Pan, X. W. Zhang, A. J. Du, D. D. Sun, J. O. Leckie, *J. Am. Chem. Soc.* **2008**, *130*, 11256 – 11257; c) B. Wang, H. B. Wu, L. Zhang, X. W. Lou, *Angew. Chem.* **2013**, *125*, 4259 – 4262; *Angew. Chem. Int. Ed.* **2013**, *52*, 4165 – 4168; d) A. Pan, H. B. Wu, L. Yu, X. W. Lou, *Angew. Chem.* **2013**, *125*, 2282 – 2286; *Angew. Chem. Int. Ed.* **2013**, *52*, 2226 – 2230; e) X. W. Lou, Y. Wang, C. L. Yuan, J. Y. Lee, L. A. Archer, *Adv. Mater.* **2006**, *18*, 2325 – 2329.
[5] J. Li, H. C. Zeng, *J. Am. Chem. Soc.* **2007**, *129*, 15839 – 15847.
[6] a) X. Chen, S. S. Mao, *Chem. Rev.* **2007**, *107*, 2891 – 2959; b) D. H. Chen, F. Z. Huang, Y. B. Cheng, R. A. Caruso, *Adv. Mater.* **2009**, *21*, 2206 – 2210; c) D. H. Chen, R. A. Caruso, *Adv. Funct. Mater.* **2013**, *23*, 1356 – 1374; d) F. Sauvage, D. H. Chen, P. Comte, F. Z. Huang, L. P. Heiniger, Y. B. Cheng, R. A. Caruso, M. Graetzel, *ACS Nano* **2010**, *4*, 4420 – 4425; e) D. H. Chen, F. Z. Huang, L. Cao, Y. B. Cheng, R. A. Caruso, *Chem. Eur. J.* **2012**, *18*, 13762 – 13769; f) D. H. Chen, L. Cao, F. Z. Huang, P. Imperia, Y. B. Cheng, R. A. Caruso, *J. Am. Chem. Soc.* **2010**, *132*, 4438 – 4444.
[7] a) C. H. Rhee, J. S. Lee, S. H. Chung, *J. Mater. Res.* **2005**, *20*, 3011 – 3020; b) B. Zhao, F. Chen, X. N. Gu, J. L. Zhang, *Chem. Asian J.* **2010**, *5*, 1546 – 1549; c) B. Zhao, F. Chen, Y. C. Jiao, J. L. Zhang, *J. Mater. Chem.* **2010**, *20*, 7990 – 7997.
[8] T. Sugimoto, T. Kojima, *J. Phys. Chem. C* **2008**, *112*, 18760 – 18771.
[9] J. Biener, E. Farfan-Arribas, M. Biener, C. M. Friend, R. J. Madix, *J. Chem. Phys.* **2005**, *123*, 094705.
[10] a) H. X. Li, Z. F. Bian, J. Zhu, D. Q. Zhang, G. S. Li, Y. N. Huo, H. Li, Y. F. Lu, *J. Am. Chem. Soc.* **2007**, *129*, 8406 – 8407; b) X. F. Chen, J. B. Liu, H. Wang, Y. L. Ding, Y. X. Sun, H. Yan, *J. Mater. Chem. A* **2013**, *1*, 877 – 883; c) Z. H. Dong, X. Y. Lai, J. E. Halpert, N. L. Yang, L. X. Yi, J. Zhai, D. Wang, Z. Y. Tang, L. Jiang, *Adv. Mater.* **2012**, *24*, 1046 – 1049; d) X. Wang, M. Y. Liao, Y. T. Zhong, J. Y. Zheng, W. Tian, T. Y. Zhai, C. Y. Zhi, Y. Ma, J. N. A. Yao, Y. Bando, D. Golberg, *Adv. Mater.* **2012**, *24*, 3421 – 3425.
[11] a) W. Li, Y. Deng, Z. Wu, X. Qian, J. Yang, Y. Wang, D. Gu, F. Zhang, B. Tu, D. Zhao, *J. Am. Chem. Soc.* **2011**, *133*, 15830 – 15833; b) X. C. Wang, J. C. Yu, C. M. Ho, Y. D. Hou, X. Z. Fu, *Langmuir* **2005**, *21*, 2552 – 2559; c) J. G. Yu, Y. R. Su, B. Cheng, *Adv. Funct. Mater.* **2007**, *17*, 1984 – 1990.
[12] a) J. B. Joo, Q. Zhang, M. Dahl, I. Lee, J. Goebl, F. Zaera, Y. D. Yin, *Energy Environ. Sci.* **2012**, *5*, 6321 – 6327; b) J. B. Joo, I. Lee, M. Dahl, G. D. Moon, F. Zaera, Y. D. Yin, *Adv. Funct. Mater.* **2013**, DOI: 10.1002/adfm.201300255; c) Z. Zhang, Y. Zhou, Y. Zhang, S. Zhou, J. Shi, J. Kong, S. Zhang, *Dalton Trans.* **2013**, *42*, 5004 – 5012.

 © 2013 Wiley-VCH Verlag GmbH & Co. KGaA, Weinheim